Annual Distributions and Sources of Arctic Aerosol Components, Aerosol Optical Depth, and Aerosol Absorption

Permanent link

http://nrs.harvard.edu/urn-3:HUL.InstRepos:14121879

Share Your Story

RESEARCH ARTICLE

Key Points:
- Significant contribution from non-BC aerosols to Arctic AAOD and deposition to snow
- Anthropogenic contribution to Arctic AOD is a factor of 4 larger in spring than in summer
- Smaller size of sulfate aerosol in Arctic summer is key to reproducing AOD observations

Correspondence to:
T. J. Breider,
tbreider@seas.harvard.edu

Annual distributions and sources of Arctic aerosol components, aerosol optical depth, and aerosol absorption

Thomas J. Breider[1], Loretta J. Mickley[1], Daniel J. Jacob[1], Qiaoqiao Wang[1], Jenny A. Fisher[2], Rachel. Y.-W. Chang[3], and Becky Alexander[4]

[1]School of Engineering and Applied Sciences, Harvard University, Cambridge, Massachusetts, USA, [2]School of Chemistry, University of Wollongong, Wollongong, New South Wales, Australia, [3]Department of Earth and Planetary Sciences, Harvard University, Cambridge, Massachusetts, USA, [4]Department of Atmospheric Sciences, University of Washington, Seattle, Washington, USA

Abstract Radiative forcing by aerosols and tropospheric ozone could play a significant role in recent Arctic warming. These species are in general poorly accounted for in climate models. We use the GEOS-Chem global chemical transport model to construct a 3-D representation of Arctic aerosols and ozone that is consistent with observations and can be used in climate simulations. We focus on 2008, when extensive observations were made from different platforms as part of the International Polar Year. Comparison to aircraft, surface, and ship cruise observations suggests that GEOS-Chem provides in general a successful year-round simulation of Arctic black carbon (BC), organic carbon (OC), sulfate, and dust aerosol. BC has major fuel combustion and boreal fire sources, OC is mainly from fires, sulfate has a mix of anthropogenic and natural sources, and dust is mostly from the Sahara. The model is successful in simulating aerosol optical depth (AOD) observations from Aerosol Robotics Network stations in the Arctic; the sharp drop from spring to summer appears driven in part by the smaller size of sulfate aerosol in summer. The anthropogenic contribution to Arctic AOD is a factor of 4 larger in spring than in summer and is mainly sulfate. Simulation of absorbing aerosol optical depth (AAOD) indicates that non-BC aerosol (OC and dust) contributed 24% of Arctic AAOD at 550 nm and 37% of absorbing mass deposited to the snow pack in 2008. Open fires contributed half of AAOD at 550 nm and half of deposition to the snowpack.

1. Introduction

The Arctic has warmed by more than 1°C over the last century, a rate almost twice the global average [*Trenberth et al.*, 2007]. Annual average Arctic sea ice coverage declined at a rate of 3.6% per decade between 1979 and 2006 [*Meier et al.*, 2007]. Global climate models (GCMs) have difficulty reproducing the observed Arctic warming [*Shindell and Faluvegi*, 2009] and the rate of observed Arctic sea ice loss [*Stroeve et al.*, 2007]. Recent studies suggest that GCM simulations of Arctic warming can be improved by better accounting of aerosols and ozone as near-term (NT) climate forcing agents [*Mickley et al.*, 2004; *Law and Stohl*, 2007; *Shindell et al.*, 2007; *Quinn et al.*, 2008]. Adequate representation of aerosols and ozone in models is challenging because of their short atmospheric lifetime and complex source and sink processes. In this work we use extensive atmospheric observations from the 2007–2008 International Polar Year (IPY), together with simulations using the GEOS-Chem chemical transport model, to better understand the factors controlling the distributions of these NT forcers in the Arctic troposphere with focus on aerosols.

Arctic aerosol and ozone concentrations at the surface and in the free troposphere are frequently elevated relative to background [*Mitchell*, 1956; *Radke et al.*, 1984; *Oltmans et al.*, 2006], due to transport of pollution from the northern midlatitudes and smoke from boreal fires [*Rahn and McCaffrey*, 1980; *Radke et al.*, 1984; *Hegg et al.*, 2010]. Aerosols perturb the radiative balance of the Arctic directly by absorbing and scattering radiation and indirectly by providing a source of cloud condensation nuclei (CCN) and ice nuclei (IN) [*Twomey*, 1974; *Charlson et al.*, 1992]. Deposition of absorbing aerosols to the snowpack reduces surface albedo and accelerates snow melt [*Warren and Wiscombe*, 1980; *Clarke and Noone*, 1985; *Hansen and Nazarenko*, 2004]. Tropospheric ozone perturbs climate through absorption of both shortwave (solar) and longwave (terrestrial)

radiation. Over the Arctic the shortwave effect is amplified by the long pathlength of sunlight and the high surface albedo of snow and ice [*Mickley et al.*, 2004; *Quinn et al.*, 2008]. *Quinn et al.* [2008] used the Goddard Institute for Space Studies GCM to estimate that anthropogenic aerosols act to cool the Arctic surface in all seasons by 0.5–1.4°C, while several studies have reported that twentieth century increases in tropospheric ozone may have warmed the Arctic surface by as much as 0.4–0.5°C in the winter and spring [*Mickley et al.*, 2004; *Shindell et al.*, 2006; *Quinn et al.*, 2008]. Anthropogenic emissions have been changing rapidly in the last decades, decreasing in Europe and North America and increasing in East Asia. This could potentially have important implications for Arctic climate.

Observed concentrations of aerosols at remote Arctic surface stations peak in the late winter and early spring, a phenomonon commonly called "Arctic haze" [*Mitchell*, 1956; *Quinn et al.*, 2007]. Fast transport along isentropic surfaces, weak vertical mixing, and lack of precipitation promote European and Russian pollution influences during this time of year [*Rahn*, 1981; *Hirdman et al.*, 2010]. As sunlight returns in spring, shortwave radiative forcing becomes important [*Mickley et al.*, 1999; *Law and Stohl*, 2007]. As spring progresses, snow and ice surfaces melt, reducing the surface albedo, and the meteorological conditions that facilitate transport from midlatitudes to the remote Arctic begin to break down. The Siberian High dissipates, Arctic precipitation increases, and decreasing stratification facilitates deposition [*Shaw*, 1995; *Stohl*, 2006; *Matsui et al.*, 2011]. Aerosol concentrations at remote Arctic stations are minimum in summer [*Stohl*, 2006]. The lower concentrations of aerosols, combined with the decrease in snow and ice coverage, reduce the top of atmosphere forcing at a time when solar radiation reaches its seasonal maximum [*Quinn et al.*, 2008].

Quantification of climate forcing from aerosols and ozone in the Arctic requires an accurate representation of their seasonal distributions [*Hansen and Nazarenko*, 2004; *Quinn et al.*, 2008]. The multimodel intercomparison studies by *Shindell et al.* [2008] and *Koch et al.* [2009] indicated large discrepancies between current models and observations of black carbon (BC) and sulfate, including incorrect seasonality and order-of-magnitude errors. The 2007–2008 IPY featured an ensemble of Arctic measurement campaigns targeting aerosols and ozone, under the auspices of the Polar Study Using Aircraft, Remote Sensing, Surface Measurements and Models, of Climate, Chemistry, Aerosols, and Transport (www.polarcat.no). The detailed data from these campaigns, complementing long-term measurements from Arctic surface sites, provide a valuable resource for testing and improving models of Arctic composition. Of particular interest is the NASA Arctic Research of the Composition of the Troposphere from Aircraft and Satellite (ARCTAS) campaign [*Jacob et al.*, 2010], which covered large domains of the North American Arctic through the depth of the troposphere in two deployments in April and July 2008.

In this paper we use the GEOS-Chem global chemical transport model (CTM) to simulate the full-year distributions of aerosol and ozone concentrations in the Arctic. Our aim is to achieve an improved representation of these NT climate forcers and their natural and anthropogenic sources, as the first step toward better simulation of their climatic effects. We discuss ozone only cursorily and focus on aerosols, which have the greater radiative impact. Comparisons are presented to ARCTAS and other observations (Table 1). We place particular emphasis on the aerosol optical depth (AOD) and absorbing aerosols because of their importance for radiative forcing. Our work builds on the knowledge gained in previous GEOS-Chem studies of ARCTAS and other Arctic data that focused on specific components and seasons [*Fisher et al.*, 2010, 2011; *Alvarado et al.*, 2010; *Mao et al.*, 2010; *Wang et al.*, 2011].

2. GEOS-Chem Description

We use the GEOS-Chem CTM version v8-02-03 (http://geos-chem.org) driven by 6-hourly assimilated meteorological data from the NASA Global Modeling Assimilation Office Goddard Earth Observing System (GEOS-5) at 2° × 2.5° horizontal resolution and with 47 vertical layers.

The GEOS-Chem aerosol simulation includes BC, organic carbon (OC), sulfate-nitrate-ammonium, dust, and secondary organic aerosol (SOA). The aerosol simulation is coupled to oxidant chemistry through heterogeneous processes; aerosol effects on photolysis rates; formation of sulfate, nitrate, and SOA; and inorganic nitrate partitioning. Primary emissions of BC are mainly in hydrophobic form (80%); 50% of emitted OC is hydrophobic. An e-folding time of 1.15 days is assumed for the aging of hydrophobic BC and OC to the hydrophilic forms. Oxidation of SO_2 to sulfate aerosol takes place via OH in the gas phase and by O_3 and H_2O_2 in the aqueous phase at temperatures above 258 K [*Alexander et al.*, 2009]. The cloud volume fractions and cloud liquid water content used for the aqueous chemistry calculation in each model grid cell are taken from

Table 1. Arctic Observations (2008) Used for Model Evaluation

Site or Campaign	Type	Time Period	Location	Species Used[a]	Reference
ARCTAS[b,c,d]	Aircraft	Apr and Jun-Jul	North American Arctic	BC[e], OC[f], nss-Sulfate[g], Dust[h]	*Jacob et al.* [2010]
ICEALOT[d,i]	Ship	Mar-Apr	North Atlantic Arctic	BC, OC, nss-Sulfate	*Frossard et al.* [2011]
ASCOS[d]	Ship	Aug-Sep	High Arctic	OC, nss-Sulfate	*Chang et al.* [2011]
Pallastunturi	Surface	Full year	Finland	BC	*Hyvärinen et al.* [2011]
IMPROVE[j]	Surface	Full year	Alaska	BC[k], OC[k], Sulfate, Dust[l]	*Malm et al.* [2004]
EMEP[m]	Surface	Full year	Northern Europe	nss-Sulfate	*Lazaridis et al.* [2002]
Barrow[n,o,p]	Surface	Full year	Northern Alaska	BC, OC, nss-Sulfate	*Quinn et al.* [2000]; *Shaw et al.* [2010]
Alert	Surface	Full year	Northern Canada	BC[q], nss-Sulfate	*Sharma et al.* [2013]; *Gong et al.* [2010]
Ny-Alesund	Surface	Full year	Svalbard, Norway	BC[r]	*Eleftheriadis et al.* [2009]
WOUDC[s]	Profile	Full year	Pan-Arctic sites	Ozone	*Oltmans et al.* [2006]
AERONET[t,u]	Column	Full year	Pan-Arctic sites	Aerosol optical depth	*Holben et al.* [1998]

[a]BC (black carbon), OC (organic carbon), and nss-Sulfate (non–sea-salt sulfate).

[b]ARCTAS observations are from the DC-8 aircraft only. The observations are filtered to remove open-fire plumes (where $[CH_3CN] > 200\,ppt$) and stratospheric air (where $[O_3]/[CO] > 1.25\,mol\,mol^{-1}$ [*Hudman et al.*, 2008]). We also remove observations from south of 60°N and near Fairbanks, Barrow, and Prudhoe Bay ($< 0.5°$ from the city and below 4 km). The Jun-Jul deployment included a focus on fire plumes, and we exclude data from below 1 km on the dedicated flights on 1, 4, 5, and 9 July.

[c]Sea-salt sulfate in ARCTAS observations are removed using a threshold ratio for sea-salt SO_4^{2-}/Na^+ of 0.252, as described in *Fisher et al.* [2011].

[d]Measurements of organic aerosol are converted to carbon mass ($\mu g\,C\,m^{-3}$) using a conversion factor of 2.1 for nonurban aerosol [*Turpin and Lim*, 2001].

[e]ARCTAS BC measurements were made using a single-particle soot photometer instrument [*Kondo et al.*, 2011].

[f]ARCTAS organic aerosol measurements were made using an aerosol mass spectrometer instrument [*Jimenez et al.*, 2003].

[g]ARCTAS Observations of submicrometer aerosol sulfate mass were made with the SAGA instrumentation package [*Dibb et al.*, 2003], using a mist chamber/ion chromatograph.

[h]ARCTAS Dust mass concentrations are calculated from observed sodium and calcium ions using filters analyzed by ion chromatography. Sodium is used to remove the sea-salt calcium assuming a sea-salt Ca:Na mass ratio of 0.04. The dust mass is determined assuming a calcium to dust mass ratio of 6.8% [*Song and Carmichael*, 2001].

[i]North of 60°N only.

[j]IMPROVE (Interagency Monitoring of Protected Visual Environments) observations at Trapper Creek are made using 24 h filter measurements collected every 3 days and are available from http://vista.cira.colostate.edu/improve/.

[k]BC and OC observations at Trapper Creek are made using thermal/optical reflectance carbon analysis.

[l]Fine dust mass is estimated using the formula in *Malm et al.* [1994].

[m]EMEP (European Monitoring and Evaluation Programme) observations are available from http://ebas.nilu.no/.

[n]BC observations at Barrow are from the NOAA Global Monitoring Division (http://www.esrl.noaa.gov/gmd/aero/net/). Observations of aerosol light absorption coefficients from the Particle Soot Absorption Photometer instrument are converted to BC mass concentrations assuming a mass absorption efficiency (MAE) of $9.5\,m^2\,g^{-1}$, based on ARCTAS observations [*McNaughton et al.*, 2011].

[o]Barrow OC measurements are described in *Shaw et al.* [2010].

[p]Barrow nss-Sulfate measurements are described in *Quinn et al.* [2000].

[q]BC observations at Alert are described in *Sharma et al.* [2013]. Observations of aerosol light absorption coefficients ($\lambda = 880\,nm$) using an aethalometer instrument are converted to equivalent BC mass concentrations assuming an MAE of $19\,m^2\,g^{-1}$.

[r]BC observations at Ny-Alesund are described in *Eleftheriadis et al.* [2009]. Observations of aerosol light absorption coefficients ($\lambda = 880\,nm$) using an aethalometer instrument are converted to equivalent BC mass concentrations assuming an MAE of $15.9\,m^2\,g^{-1}$.

[s]World Ozone and Ultraviolet Radiation Data Centre (WOUDC) observations (http://www.woudc.org) for stations >65°N are Alert [62.3°W, 82.5°N], Barrow [156.6°W, 71.3°N], Eureka [85.9°W, 80.0°N], Ny-Alesund [11.8°E, 78.9°N], Resolute [94.9°W, 74.7°N], Sodylanka [26.7°E, 67.4°N], and Summit [38.5°W, 72.6°N].

[t]Aerosol Robotic Network (AERONET) stations >65°N are Andenes [16.0°E, 69.2°N], Barrow [156.6°W, 71.3°N], Hornsund [15.6°E, 77.0°N], Kangerlussuaq [50.6°W, 70°N], Ny-Alesund [11.8°E, 78.9°N], OPAL [85.9°W, 79.9°N], PEARL [86.4°W, 80.0°N], Resolute Bay [94.9°W, 74.7°N], and Thule [68.7°W, 76.5°N]. We include an observation point only if six or more stations have data for that month.

[u]The model AOD is sampled at 550 nm. The observed AOD at 440 nm is corrected for 550 nm using the Angstrom exponent and assuming a linear fit [*Seinfeld and Pandis*, 2006].

Table 2. Global BC, OC, SO_2, NH_3, and Dust Emissions in GEOS-Chem for 2008

Species	Emission Source	Europe	China	North America	Russia	Global
BC (Tg C yr^{-1})	Anthropogenic[a]	0.59	2.64	0.37	0.24	7.04
	Open fires	0.23	0.24	0.02	0.67	11.15
OC (Tg C yr^{-1})	Anthropogenic[a]	1.04	4.96	0.53	0.51	14.5
	Open fires	1.28	2.18	0.96	6.03	82.85
SO_2 (Tg S yr^{-1})	Anthropogenic[a]	5.19	16.22	8.11	2.45	62.93
	Open fires	0.03	0.08	0.03	0.27	1.90
	Volcanoes					13.3
	Oceanic DMS					17.14
NH_3 (Tg N yr^{-1})	Anthropogenic[a]	4.83	11.23	2.56	1.13	38.6
	Open fires	0.15	0.24	0.08	0.70	9.4
	Other natural[b]					14.3
Dust (Tg yr^{-1})	Natural					1107

[a]Includes emissions from fossil fuel and biofuel combustion.
[b]Includes oceanic, soil, and agricultural emissions.

GEOS-5 assimilated meteorological fields. A small fraction of SO_2 from anthropogenic sources is emitted as particulate sulfate to account for subgrid-scale processes. Dimethylsulfide (DMS) oxidation takes place via reaction with OH and NO_3. A detailed description of the basic model is provided by *Mao et al.* [2010] for ozone chemistry, by *Fisher et al.* [2011] for sulfate-nitrate-ammonium aerosol chemistry, and by *Wang et al.* [2011] for carbonaceous aerosols. These studies presented detailed comparisons with ARCTAS and other observations. For dust aerosol we use the simulation described by *Fairlie et al.* [2007], adapted for GEOS-5 meteorology by *Fairlie et al.* [2010]. The GEOS-Chem sea-salt aerosol simulation is described by *Alexander et al.* [2005]. SOA formation takes place via the reversible condensation of the oxidation products of biogenic and aromatic volatile organic compounds [*Henze and Seinfeld*, 2006], as well as the irreversible condensation of glyoxal and methyl glyoxal [*Fu et al.*, 2008, 2009]. Aerosol optical properties are described in *Drury et al.* [2010], with updated dust size distribution from *Ridley et al.* [2012].

Wet deposition of aerosol in GEOS-Chem takes place in convective and large-scale precipitation through in-cloud and below-cloud scavenging, as well as in convective updrafts. For below-cloud scavenging, we use the parameterization from [*Feng*, 2007, 2009]. For sulfate and carbonaceous aerosols, we assume scavenging coefficients specific to accumulation mode sized particles and coarse mode coefficients for sea salt and dust. Scavenging coefficients are dependent on the phase of precipitation, where snow ($T < 268$ K) scavenging is more efficient than rain ($T > 268$ K) due to the larger cross-sectional area of snow crystals. In-cloud scavenging includes the removal of aerosols that act as CCN and IN. We assume 100% of hydrophilic aerosol are scavenged in warm and mixed phase clouds ($T > 268$ K). In cold clouds ($T < 268$ K) only hydrophobic BC and dust are scavenged. Dry deposition of aerosol is based on a standard resistance in-series scheme [*Wesely*, 1989] and assumes an aerosol dry deposition velocity of 0.03 cm s^{-1} over snow and ice surfaces [*Nilsson and Rannik*, 2001]. A detailed description of the aerosol scavenging parameterization in GEOS-Chem is provided in *Wang et al.* [2011]. We conduct a full-year simulation of this coupled aerosol-ozone system for 2008 with 6 months of initialization in 2007. We use sensitivity simulations to separate natural and anthropogenic contributions. For the purpose of this analysis, open fires are considered natural.

Anthropogenic emissions of nitrogen oxides ($NO_x \equiv NO + NO_2$), sulfur oxides ($SO_x \equiv SO_2 +$ sulfate), and CO are from *van Donkelaar et al.* [2008], updated to 2008 and with modifications to SO_x emissions from *Fisher et al.* [2011]. Anthropogenic carbonaceous aerosol emissions are from *Bond et al.* [2007] for the year 2000. BC and primary OC emissions from anthropogenic sources in Asia and Russia are doubled to match surface BC observations in China and in the Arctic as described by *Wang et al.* [2011]. The increase is consistent with industrial growth in China and the economic recovery in Russia since the year 2000. Table 2 summarizes the aerosol emissions in our study, with a focus on the source regions most relevant for transport to the Arctic. Global anthropogenic BC emissions in our study are 7.04 Tg C yr^{-1}, higher than the 5.14 Tg C yr^{-1} emissions used by *Bourgeois and Bey* [2011] but within the emission range of 3.13–10.08 Tg C yr^{-1} estimated by *Bond et al.* [2004]. The annual Chinese BC emission of 2.64 Tg C in our study is also larger than recent estimates, but within the range of uncertainty [*Lu et al.*, 2011]. We do not account for seasonality in Asian BC emissions. Anthropogenic emissions of OC, SO_2, and NH_3 are all in agreement with previous studies [*Bond et al.*, 2007; *Smith et al.*, 2011].

Table 3. Global Annual Mean Burdens, Lifetime, Total Deposited Mass, and Fraction of Removal by Wet and Dry Deposition for GEOS-Chem Aerosols[a]

Species	Burden (Tg)	Lifetime (days)	Total Deposition (Tg species yr^{-1})	Wet (%)	Dry (%)
BC	0.27	5.38	18.1	73	27
OC	1.93	5.48	128.9	76	24
Sulfate	0.39	3.57	40.34	89	11
Dust	10.32	1.71	2206	54	46

[a]Values are integrated over the troposphere column between the surface and 300 hPa.

Fire emissions are from the Fire Locating and Monitoring of Biomass Emissions (FLAMBE) inventory [*Reid et al.*, 2009]. We apply modifications to Eurasian fire sources to match ARCTAS observations of CO, BC, and OC [*Fisher et al.*, 2010; *Wang et al.*, 2011]. The FLAMBE emissions from Russia and Southeast Asia are scaled down by 47% and 55%, respectively, following the analysis of ARCTAS CO observations in *Fisher et al.* [2010]. *Wang et al.* [2011] found that the Russian OC emission factor should also be reduced to 6.8 g carbon per kilogram dry mass burned to match ARCTAS OC observations. In addition, we decrease North American fire emissions by 0.375 relative to FLAMBE to match ARCTAS CO observations as suggested by *Alvarado et al.* [2010]. *Kondo et al.* [2011] found an average BC:CO emission ratio of 2.3 ng m^{-3} ppbv^{-1} CO for North American fires based on ARCTAS data, and we adopt that value here. Annual BC and OC emissions from boreal regions (45°N to 65°N) are 0.86 Tg C yr^{-1} and 7.59 Tg C yr^{-1}, respectively. Boreal fires were unusually extensive in Eurasia in spring 2008 [*Fisher et al.*, 2010], while summer was more typical [*Jacob et al.*, 2010].

The GEOS-Chem simulation of *Fisher et al.* [2011] showed a factor of 2 overestimate in sulfate mass concentrations in April at Barrow and in May at Denali in Alaska. Our initial analysis found this model sulfate bias to extend into summer. We implement here several improvements to the simulation of Arctic sulfate. These include an improved treatment of cloud pH and hence aqueous-phase oxidation of SO$_2$ by ozone in clouds as described in *Alexander et al.* [2012], an update of the dimethylsulfide (DMS) seawater climatology following *Lana et al.* [2011], and inclusion of the unit-yield formation of dimethylsulfoxide (DMSO) from the addition-pathway oxidation of DMS by OH [*Barnes et al.*, 2006]. As will be shown below, the update to the aqueous oxidation chemistry reduces the model spring bias at Zeppelin and Barrow. The use of the new DMS seawater climatology [*Lana et al.*, 2011] results in a 40% decrease in DMS emissions in the Arctic spring and summer because of lower DMS seawater concentrations in the region. The inclusion of DMSO chemistry reduces the yield of sulfate formation from the oxidation of DMS. Due to its high solubility, DMSO is efficiently scavenged and oxidized in cloud droplets to meathanesulphonicacid. These updates to the DMS emissions and oxidation reduce the model bias in summer at Zeppelin and Alert.

Table 3 shows the simulated global burden and lifetime and deposition budgets for each of the aerosol species. The simulated BC lifetime is within the range of Aerosol Comparisons between Observations and Models (AEROCOM) values reported by *Koch et al.* [2009]. We have a larger global BC burden than most AEROCOM models; however, this is the result of the high open-fire emissions in the tropics in the FLAMBE inventory, a region that has little importance for the Arctic. Table 4 shows the simulated Arctic burdens, lifetimes, and deposition fluxes for the aerosol species in our study. The lifetimes of BC and sulfate aerosol in the Arctic are longer than those reported by previous studies [e.g. *Bourgeois and Bey*, 2011]. We refer the reader to *Wang et al.* [2011, section 5] for a detailed discussion of differences in emissions and deposition parameterizations between GEOS-Chem and previous global model studies of aerosols in the Arctic.

Table 4. Annual Mean Burdens, Lifetimes, Total Deposited Mass, and Fraction of Removal by Wet and Dry Deposition for GEOS-Chem Aerosol in the Arctic[a]

Species	Burden (Gg)	Lifetime (days)	Total Deposition (Tg yr^{-1})	Wet (%)	Dry (%)
BC	6.46	8.27	0.28	89	11
OC	42.6	6.25	2.49	90	10
Sulfate	25.4	8.34	1.11	91	9
Dust	108.4	2.43	16.3	93	7

[a]Values are integrated over the Arctic troposphere column between the surface and 300 hPa for latitudes greater than 65°N.
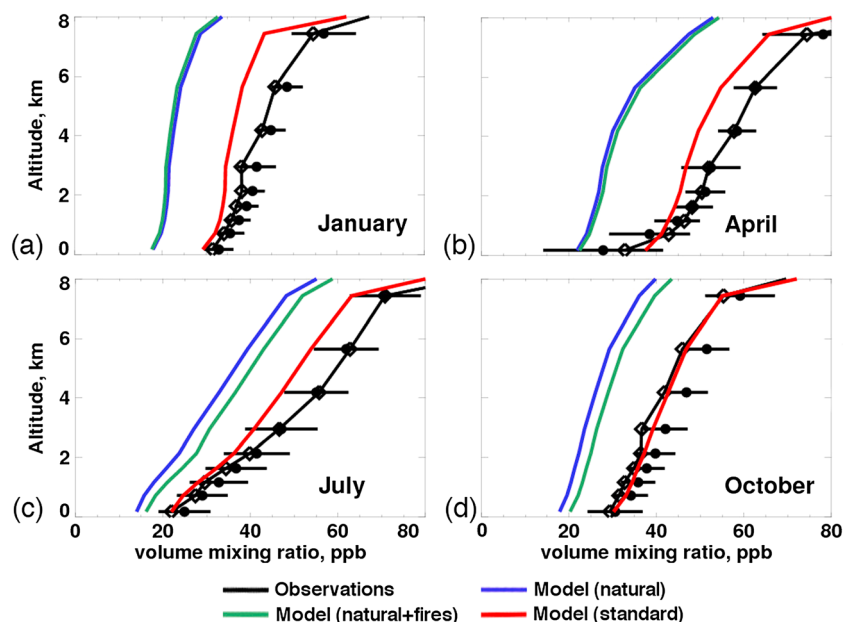
Figure 1. Vertical profiles of monthly ozone volume mixing ratios over the Arctic in different seasons for 2008. Observations averaged over the seven WOUDC sites north of 65°N (Table 1) are compared to GEOS-Chem values for the standard simulation, a sensitivity simulation with no anthropogenic emissions (natural + fires) and a sensitivity simulation with no anthropogenic or fire emissions (i.e., natural). Horizontal bars for the observed profiles indicate the ±1 standard deviations for 2000–2009. Open circles show the 2008 observations, and the solid circle shows the 2000–2009 mean.

Figure 1 compares observed and simulated monthly mean ozone profiles for different seasons of 2008, averaged across seven stations in the WOUDC (World Ozone and Ultraviolet Radiation Data Centre) (http://www.woudc.org/) database north of 65°N. The model has no bias near the surface but underestimates ozone by 5–10 ppb in the middle and upper troposphere for all seasons except fall. Observed concentrations increase by 14 ppb on average from January to April due to photochemical production [*Browell et al.*, 2003], and this is well reproduced by the model. The model underestimate in summer is consistent with the previously reported underestimate of peroxyacetylnitrate [*Alvarado et al.*, 2010] and suggests insufficient photochemical production from Asian pollution and boreal fires.

We conducted sensitivity simulations to examine the model enhancement of ozone due to open fires and human influence. The blue lines in Figure 1 show values for a sensitivity simulation excluding fires and anthropogenic sources, while the green lines are for a simulation excluding only anthropogenic sources. The anthropogenic enhancement is maximum in April (19 ppb) and minimum in August (10 ppb). The open-fire enhancement is 4 ppb in August but only 1 ppb in April.

3. Aerosol Distributions

We examine in this section the observed distributions of different aerosol components over the Arctic, the ability of GEOS-Chem to reproduce these distributions, and the implications for source attribution. Figure 2 shows simulated and observed seasonal mean aerosol concentrations in surface air over the Arctic in spring and summer, when the radiative impact is maximum [*Flanner et al.*, 2007; *Quinn et al.*, 2008]. GEOS-Chem values (background) are compared to observations (circles). Aerosol concentrations are generally lower in summer than in spring, for reasons discussed in section 1. We discuss below the results of Figure 2 as well as other features of the distribution for each component.

3.1. Black Carbon

Figure 3 shows the seasonality of BC concentrations at Barrow and Trapper Creek in Alaska, Alert in Nunavut, Canada [*Sharma et al.*, 2013], Ny-Alesund in Svalbard, Norway [*Eleftheriadis et al.*, 2009], and Pallas in Finland [*Hyvärinen et al.*, 2011]. Observations at Barrow are from the NOAA Global Monitoring Division (http://www. esrl.noaa.gov/gmd/aero/net/), and observations at Trapper Creek are from the Interagency Monitoring of
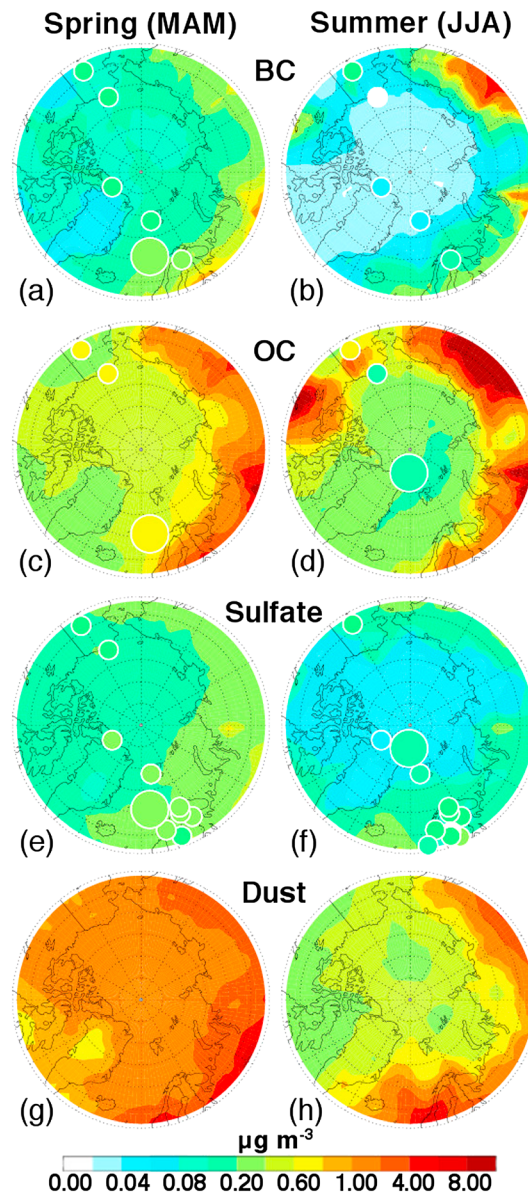
Figure 2. Seasonal mean surface air concentrations of (a and b) black carbon (BC), (c and d) organic carbon (OC), (e and f) sulfate, and (g and h) dust aerosol in the Arctic in spring (March-April-May) and summer (June-July-August) 2008. Small circles indicate observations at surface sites, and large circles show cruise data, including the spring ICEALOT campaign (> 60°N) in March and April 2008 and the summer ASCOS campaign in August and September 2008. GEOS-Chem results are shown as background contours. The observations are further described in Table 1.

Protected Visual Environments (IMPROVE) network (http://vista.cira.colostate.edu/improve/). Observed concentrations at Barrow, Alert, Ny-Alesund, and Pallas show a maximum in late winter-early spring attributable to anthropogenic sources in Eurasia [*Wang et al.*, 2011]. The summer minima at these stations reflect slower transport and increased scavenging, particularly at the more remote Barrow, Alert, and Ny-Alesund sites. At Trapper Creek in central Alaska, observed BC concentrations in February and March are half those at Barrow because the Brooks mountain range blocks long-range transport from Eurasian sources [*Quinn et al.*, 2002]. In late spring-summer, by contrast, BC concentrations are higher at Trapper Creek than at Barrow due to larger year-round influence of North American anthropogenic BC source. The model provides a good match to observations. Data from the International Chemistry Experiment in the Arctic Lower Troposphere (ICEALOT) cruise [*Frossard et al.*, 2011] in spring (Figure 2a) indicate a mean concentration of $0.27 \pm 0.13\ \mu g\ m^{-3}$ north of 60°N, as compared to a simulated value of $0.12 \pm 0.05\ \mu g\ m^{-3}$ sampled along the cruise track for the corresponding days.

Figure 4a compares BC model results with mean vertical profiles from the ARCTAS April and July campaigns. Values are lower in July than in April throughout the tropospheric column. The high values in the midtroposphere in April are due to a combination of Asian anthropogenic and Russian fire influences transported to the Arctic in warm conveyor belts [*Wang et al.*, 2011]. The observations in July are less than $0.025\ \mu g\ m^{-3}$ throughout the vertical profile, but the model shows an increase with altitude due to long-range transport of deep convective outflow from Asian pollution (summer monsoon) and Siberian fire plumes. A more recent version of GEOS-Chem corrects this problem by increasing the scavenging efficiency of BC in deep convection [*Wang et al.*, 2014].

Figure 5a gives a summary of the model representation of Arctic BC concentrations vs. altitude and season. In winter, elevated concentrations are confined below 2 km and have a dominant Russian source [*Wang et al.*, 2011]. Peak tropospheric loadings are in spring, when the model provides a good match to the ARCTAS observations. Minimum BC concentrations are in October after the fire season and before the efficient wintertime transport of pollution develops. Sensitivity simulations indicate that the anthropogenic influence is largest in March, when it contributes 70% of the Arctic BC burden, dropping to 40% in May and 10% in summer-fall.
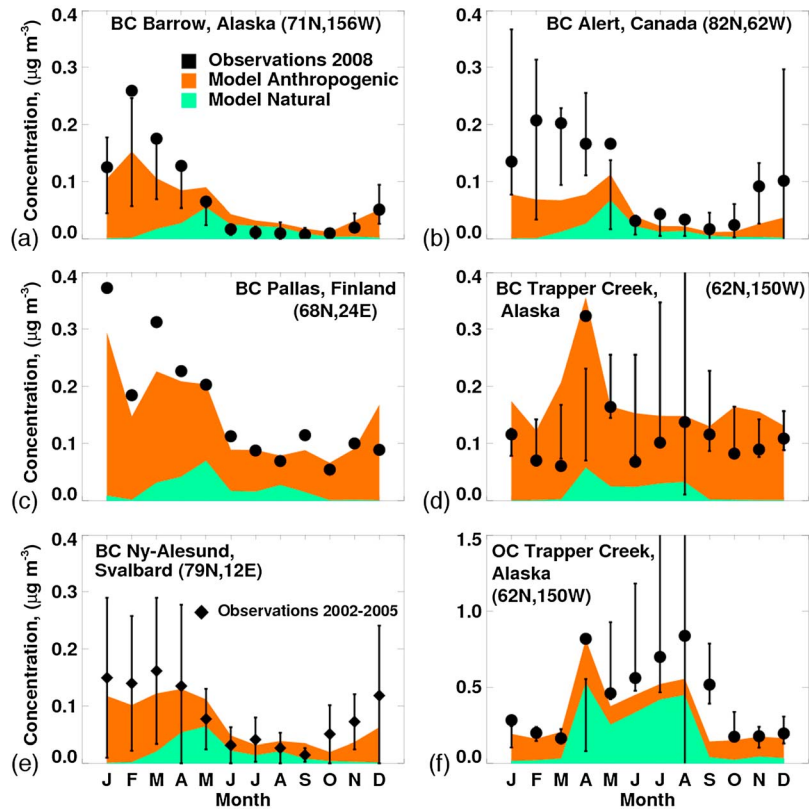
3.2. Organic Carbon

Observations of organic aerosol in the high Arctic show a factor of 5 decrease from spring to summer, as shown in Figure 2 with the ICEALOT and the Arctic Ocean Cloud Ocean Study (ASCOS) cruises [*Chang et al.*, 2011] and

Figure 3. Seasonal variation of BC and OC aerosol concentrations at Arctic sites in 2008. Observations for 2008 are shown as black symbols, and vertical bars show the interannual standard deviation of monthly mean concentrations for 2001–2009 at (a) Barrow, (b) Alert, and (d and f) Trapper Creek. (c) Pallas has observations for only 2008 and 2009. (e) Observations at Ny-Alesund are for the period 2002–2005 only; the diamond symbol shows the interannual mean. Model values are shown as stacked contours for natural (green) and anthropogenic (red) contributions.
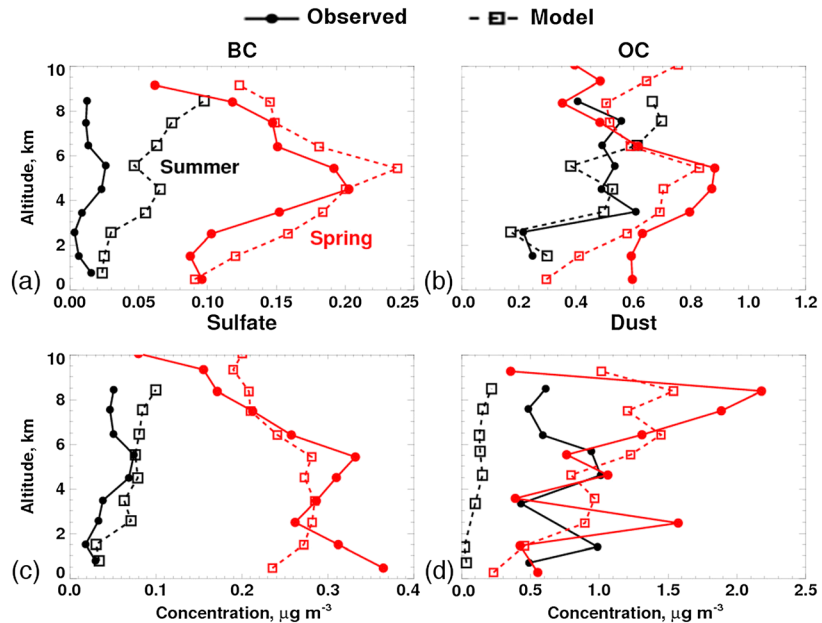
Figure 4. (a–d) Log-mean vertical profiles of aerosol mass concentrations during the ARCTAS campaign over the North American Arctic in April (red lines) and July (black lines) 2008 [*Jacob et al.*, 2010]. Observations are from the DC-8 aircraft. Observations are screened as described in Table 1. GEOS-Chem model results are sampled along the flight tracks and for the flight times.
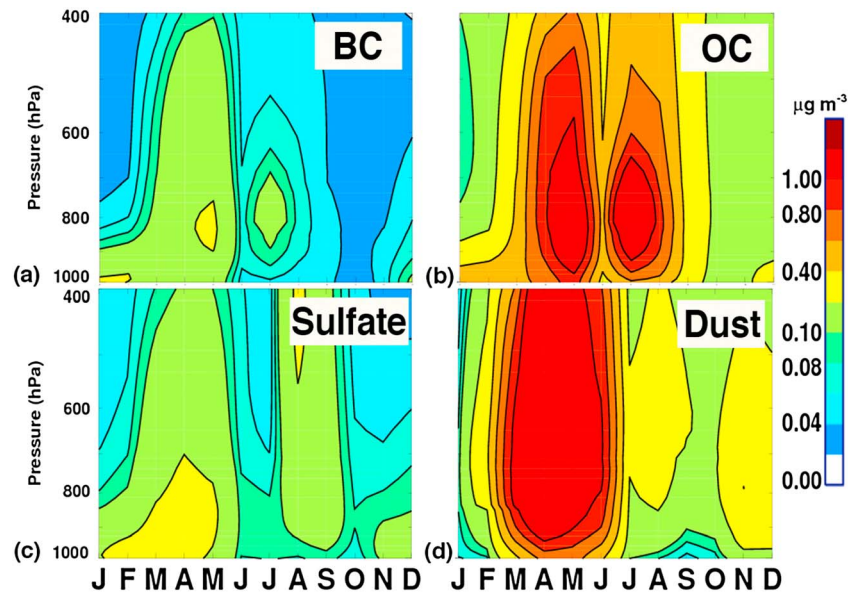
Figure 5. (a–d) Mean vertical profiles of aerosol mass concentrations in the Arctic (north of 65°N). Values are GEOS-Chem model results for 2008.

at Barrow, Alaska [*Shaw et al.*, 2010]. At Barrow, the model shows a small 10% spring-summer decrease in OC, as shown in Figure 2, apparently because of an overestimate of fire influence in summer. Observations at Trapper Creek (Figure 3f) show seasonal peaks in April and in summer, reflecting the influence of Russian fires (April) [*Warneke et al.*, 2009, 2010] and of North American fires (summer). The model reproduces these features and finds fires to be the main source of OC in spring and summer.

The ARCTAS vertical profiles (Figure 4b) show that higher concentrations in spring than in summer extend up to 6 km, above which the difference vanishes. The model provides an overall good simulation, although it is too low near the surface in spring and too high in the upper troposphere in summer. As for BC, the elevated concentrations in the midtroposphere in April are due to Siberian fires [*Wang et al.*, 2011]. Concentrations remain relatively high in summer throughout the tropospheric column, reflecting emissions from North American fires below 2 km and Siberian fire influences above 3 km. The pan-Arctic model perspective in Figure 5b shows prominent peaks in spring and summer due to fires, extending through the depth of the tropospheric column. Thus, we find that the relatively high free tropospheric concentrations observed by ARCTAS in July are representative of the wider Arctic. The model overestimate of fire influence in surface air over the high Arctic in summer (Figure 2d) could reflect insufficient scavenging or lofting of fire plumes.

Open fires account for 70% of Arctic OC in the model throughout the troposphere from April through August. Anthropogenic emissions (mostly primary OC from combustion) are important in the Arctic boundary layer from November through March, providing $0.2–0.6\,\mu g\,m^{-3}$ during that period. SOA (90% biogenic in the model) contributes up to 30% of total surface OC in late summer and early fall. The simulated annual contributions to Arctic tropospheric OC are 53% from fires, 29% from biogenic SOA, and 18% from anthropogenic sources.

3.3. Sulfate

Arctic sulfate concentrations in surface air show a similar seasonal pattern to BC, with the model successfully representing the geographical distribution in the observations and the decrease from spring to summer (Figures 2 and 2f). Here and elsewhere we show and discuss only the non–sea-salt component of sulfate.

Figure 6 shows the seasonal variation at four Arctic sites. The seasonality in the high Arctic is driven by the large anthropogenic influence in winter and spring, when sources from Russia and Kazakhstan (winter) and East Asia (spring) are most important [*Fisher et al.*, 2011]. The model is consistent with observations but is too low at Alert in winter and spring, as discussed by *Fisher et al.* [2011]. Observed sulfate concentrations in February and March at Trapper Creek are a factor of 2–3 lower than at Barrow and Alert for the same reason as for BC (section 3.1). Anthropogenic sources are important in winter and early spring, providing 83% of the
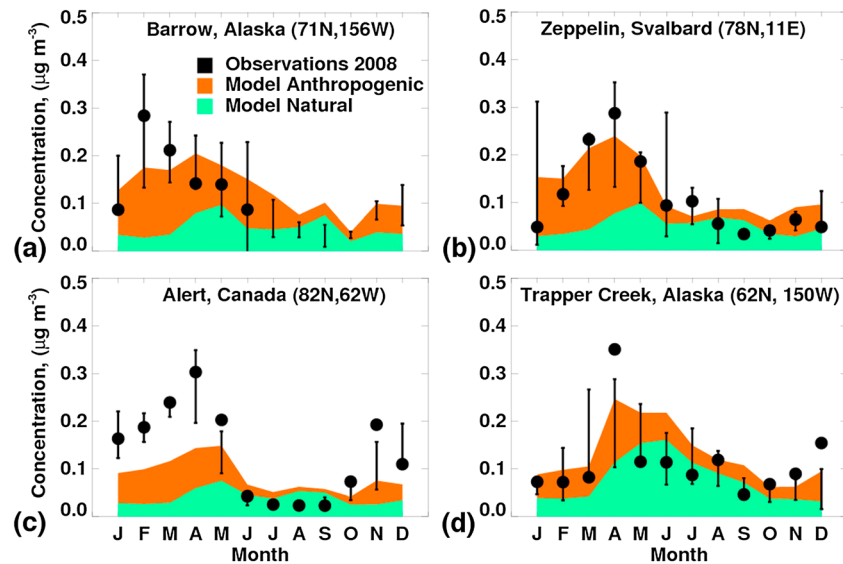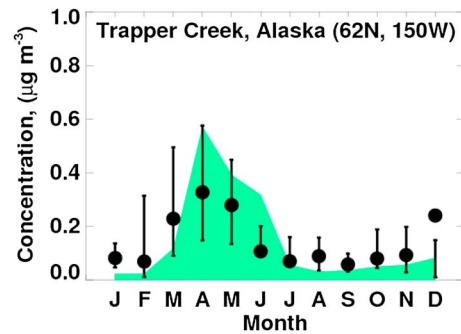
Figure 6. Mean seasonal variation of sulfate aerosol concentrations at Arctic sites in 2008. Observations for 2008 are shown as black symbols, and vertical bars show the interannual standard deviation for the period 1997–2008 at Barrow, 1999–2008 at Zeppelin, 1998–2008 at Alert, and 2001–2009 at Trapper Creek. The observations are further described in Table 1. Model values are shown as stacked contours for natural (green) and anthropogenic (red) contributions.

total Arctic surface sulfate at that time of year. The natural sulfate in winter and spring at Trapper Creek is from volcanic sources. The seasonality in the anthropogenic source contribution is consistent across all sites with the exception of Barrow in summer, where the elevated anthropogenic influence is driven by emissions from the Prudhoe Bay oil field, as shown in Figure 2f by the higher sulfate concentrations on the northern coast of Alaska. Volcanic emissions drive the maxima in simulated natural sulfate in spring and late summer at Barrow, Zeppelin, and Alert. The marine biogenic source of sulfate shows a broad summer maximum.

ARCTAS observations in Figure 4c show a 70% decrease in the column average sulfate between spring and summer, with little vertical gradient, and this is reproduced in the model. *Fisher et al.* [2011] pointed out that different sources of sulfate dominate at different altitudes in spring. We find the same in summer with oceanic DMS dominating below 2 km, volcanic and anthropogenic sources both important between 2 and 6 km, and anthropogenic sources dominant above 6 km. We find that the main anthropogenic component in summer is from East Asia, whereas in spring there are also major contributions from Europe and North America [*Fisher et al.*, 2011].

Figure 5c shows that elevated sulfate concentrations in the model are confined close to the surface in January and February but extend throughout the troposphere in spring. The Arctic column sulfate burden in late spring is a mixture of anthropogenic and natural sources [*Fisher et al.*, 2011]. The peak in sulfate in the free troposphere in late summer is the result of volcanic emissions from the Kasatochi eruption in the Aleutian Islands and was observed in AOD measurements at Ny-Alesund, Svalbard [*Hoffmann et al.*, 2010], and at Barrow [*Tomasi et al.*, 2012]. During this time we estimate that volcanic emissions increased the Arctic tropospheric sulfate burden by a factor of 3 compared to those in July. The simulated 2008 annual contributions to Arctic tropospheric sulfate are 48% from anthropogenic sources, 30% from volcanic sources, 19% from DMS, and 3% from fires. The anthropogenic influence is largest in March when it contributes 60% of the Arctic sulfate burden. It drops to 30% in summer-fall.

Fisher et al. [2011] found from the ARCTAS observations and GEOS-Chem simulations that the sulfate aerosol is acidic throughout the Arctic troposphere in winter-spring. We find that the summer aerosol is more acidic in the boundary layer compared to that of spring, due to sulfate production from DMS. In the free troposphere the summer aerosol is almost neutralized because boreal fires provide a large source of NH_3. *Fisher et al.* [2011] showed that nitrate contributed <15% to the total aerosol anion concentration during ARCTAS in April. We find that below 5 km the simulated nitrate contribution remains less than 15% in the spring and summer months, with the exception of July when it increases to 20–30% in response to large fire emissions at that

Figure 7. Seasonal variation of fine mode dust aerosol (<2.5 μm diameter) concentrations at Trapper Creek, Alaska, in 2008. Observations for 2008 are shown as black symbols, and vertical bars show the interannual standard deviation for the period 2001–2009. The observations are further described in Table 1. Model values are shown as green contours.

time. The nitrate contribution is most important above 5 km in June and July, when it provides 40% to total simulated aerosol anion concentration.

3.4. Dust

Surface observations of dust at Trapper Creek (Figure 7) show peak values in spring. This spring peak extends to the entire Arctic and to all altitudes (Figures 2 and 5d). We estimate the source contribution from the Sahara and the Taklamakan and Gobi deserts using two sensitivity simulations with dust emissions from these regions independently switched off. Source attribution at Trapper Creek in the model shows that 60% of dust in spring is from the Sahara, 22% from the Taklamakan and Gobi deserts, and 18% from other deserts. Dust emissions from dry valleys in Greenland and from Iceland may also contribute to the Arctic dust budget. Elemental analysis of the dust observations at Trapper Creek suggests a Saharan influence only during mid-May (Al:Ca >3.8, [*Perry et al.*, 1997]). ARCTAS vertical profiles in spring (Figure 4d) show an increase with altitude and good consistency between model and observations. We find that the upper tropospheric maximum is mainly of Saharan origin. The simulated dust concentrations in summer are an order of magnitude lower than in spring as a result of weaker transport to the Arctic and increased precipitation. This sharp seasonal decrease is seen in the surface observations at Trapper Creek, but the ARCTAS observations show little decrease. The ARCTAS summer flights were mostly over West Central Canada, and dust concentrations there were comparable to observations at the two IMPROVE sites in North Dakota (averaging $0.69\,\mu g\,m^{-3}$ for July 2008). Previous aircraft observations over the Great Plains in summer from the SUbsonic aircraft Contrail & Clouds Effects Special Study (SUCCESS) campaign showed elevated dust concentrations throughout the tropospheric column reflecting regional convective lifting [*Talbot et al.*, 1998]. The model underestimate of dust concentrations over the North American Great Plains in summer has been noted before in a GEOS-Chem simulation by *Fairlie et al.* [2007] and suggests a missing dust source in that region and season. The dust source in GEOS-Chem is confined to topographic depressions in desert areas [*Ginoux et al.*, 2001]. A broader definition of dust-producing regions as in the Dust Entrainment and Deposition model [*Zender et al.*, 2003] would better represent the North American dust source in summer but lead to model overestimates in other seasons [*Fairlie et al.*, 2007]. One ARCTAS summer flight to the remote Arctic over Greenland on 9 July still observed dust concentrations greater than $0.5\,\mu g\,m^{-3}$ above 4 km. Better understanding is needed of that North American dust source in summer.

The magnitude of Saharan influence in the Arctic is uncertain. We find in our model that the Sahara is responsible for 65% of total dust in the Arctic on an annual mean basis. Chemical and back-trajectory analyses point to evidence of transport of Saharan dust to the Arctic either through transport across Northern Europe or around the Bermuda High [*Franzén et al.*, 1994; *Ansmann et al.*, 2003; *Rodríguez et al.*, 2012; *VanCuren et al.*, 2012]. However, *Bory et al.* [2003] found no evidence of Saharan origin in isotopic and mineralogical dust analysis of Greenland snow samples.
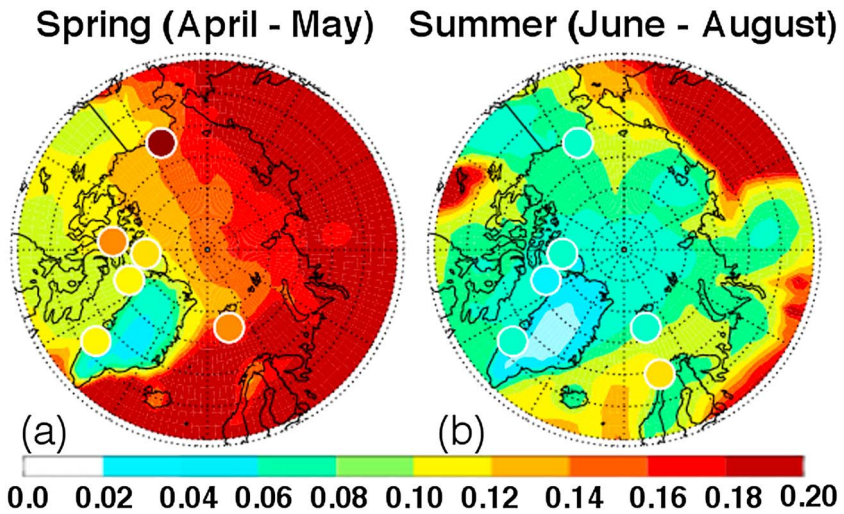
4. Aerosol Optical Depth

Figure 8 shows the spatial distribution of 550 nm aerosol optical depth (AOD) over the Arctic in spring and summer. Model results (background) are compared to sun photometer observations from Arctic Aerosol Robotics Network (AERONET) stations [*Holben et al.*, 1998]. AOD provides an integrated measure of aerosol abundances that is most relevant for aerosol scattering of radiation. The model captures the seasonal decrease in Arctic AOD from spring to summer. Simulated AODs are higher in the Eurasian Arctic than the North American Arctic, but there are insufficient AOD observations in Eurasian Arctic in 2008 to evaluate this result. Figure 9a shows the mean seasonal variation of AOD at the AERONET sites, where observations are limited to March–October because of winter darkness. The observations show an April-May maximum, and this is captured by the model. There is a secondary September maximum in 2008, both in the observations

Figure 8. Seasonal mean aerosol optical depth (AOD) at 550 nm over the Arctic in (a) spring (April-May) and (b) summer (June–August) 2008. GEOS-Chem model values are shown as background contours. Observations from the AERONET network [*Holben et al.*, 1998] for stations north of 65°N are shown as circles.

and the model, due to the eruption of the Kasatochi volcano in the Aleutian Islands on 8 August. The larger observed AOD perturbation (from the multiannual mean) in September than in August is due to the relatively long lifetime of SO_2 against oxidation to sulfate in the upper troposphere and lower stratosphere (weeks) [*Kravitz et al.*, 2010]. The simulation reproduces well the monthly observed AOD in 2008 at the Arctic stations north of 65°N ($R^2 = 0.56$, significant at the 95% confidence level). The AERONET climatological record, also shown in Figure 9a, is relatively flat from June to October. The model suggests that AODs are minimum in December-January, but this is inconsequential from a radiative forcing perspective because of the low availability of shortwave radiation in the Arctic at this time.

We find that successful simulation of the observed seasonal variation of Arctic AOD in the model is contingent on accounting for the observed seasonal shift in sulfate aerosol size [*Bodhaine et al.*, 1981; *Quinn et al.*, 2002; *Engvall et al.*, 2008]. An initial simulation using fixed aerosol optical properties from GEOS-Chem [*Drury et al.*, 2010]—i.e., a lognormal distribution with a geometric mean radius of 70 nm for sulfate—overestimated the observed Arctic AODs in summer by a factor of 2. Observations show that the geometric mean radius of sulfate particles decreases from 80 nm in spring to approximately 25 nm in summer, reflecting a decrease in transport of aged particles from midlatitudes and an increase in local biogenic sulfur emissions, photochemistry, and
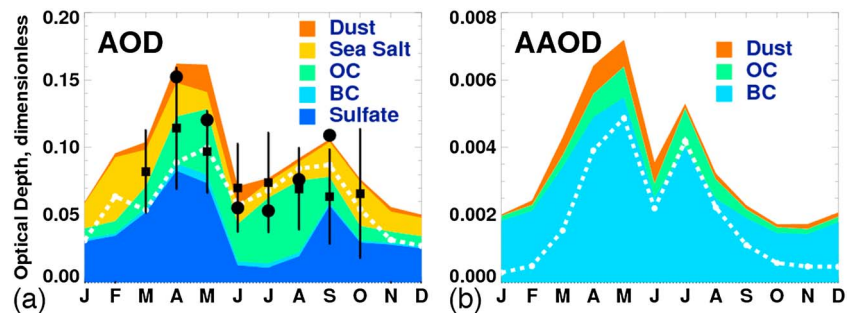
Figure 9. (a) Seasonal variation of Arctic AOD at 550 nm averaged across the eight Arctic AERONET stations (also see Table 1 for listing). The black circles show observations for 2008. The vertical bars indicate the interannual standard deviation for the period 1999–2011, and the horizontal bar shows the interannual mean. GEOS-Chem model values are shown as stacked contours with individual contributions from sulfate, BC, OC, sea salt, and dust. The white dashed line shows the total contribution from natural sources in the model. There are no AERONET data between November and February and only sparse data in October. (b) Seasonal variation of Arctic absorption aerosol optical depth (AAOD) at 550 nm north of 65°N. Values are GEOS-Chem model results for 2008. The stacked contours show the BC, OC, and dust contributions. The white dashed line shows the total contribution from natural sources.

nucleation [*Ström et al.*, 2003; *Engvall et al.*, 2008]. The size transition happens between late May and early June each year [*Engvall et al.*, 2008]. The smaller summertime particles scatter visible radiation less efficiently. To account for the seasonal shift to smaller particles, we reduce the mean sulfate particle size in GEOS-Chem by a factor of 3 between June and August throughout the Arctic (north of 65°N). This results in a factor of 3.4 decrease in sulfate AOD. The reduction in the sulfate particle size is applied only to the calculation of the AOD; no feedbacks on aerosol scavenging are accounted for. Through accounting for the observed size shift to smaller particles in Arctic summer, we can better estimate the climate impact of the aerosol. Models that do not consider this size shift will overestimate the sulfate component of the AOD in Arctic summer and may draw incorrect conclusions about aerosol forcing in the region at this time of year.

We see from Figure 9a that the dominant contributors to the AOD in the Arctic are sulfate, OC, and sea salt. Sulfate accounts for 50% of the model AOD except in summer when OC from fires is more important. Sea salt is most important in fall and winter when it accounts for 30–40% of AOD. The April-May seasonal peak in AOD is due to both anthropogenic sulfate and OC from fires, and the long-term AERONET record shows that this is a robust climatological feature as shown by the error bars in Figure 9a. The exceptional Eurasian fires in early spring 2008 are evident in April.

The white line in Figure 9a shows the natural contribution to model AOD including biogenic, volcanic, dust, fire, and sea-salt sources. We see that most of the AOD is natural in all seasons. The largest anthropogenic influence is in April-May when it increases the AOD by 0.07. Sulfate aerosols represent 84% of the total anthropogenic AOD in April-May, with OC contributing 12% and BC 4%. The larger anthropogenic sulfate AOD in spring compared to that in winter is not as evident at the surface sites in Figure 6 but is manifest in the ARCTAS aircraft data of Figure 4. The natural Arctic AOD is a mixture of sources with fires contributing 25% on an annual mean basis, sea salt 23%, natural sulfate 18%, and dust 7%. All of these natural sources are subject to potential feedback from climate change. For example, melting Arctic sea ice would increase the source of sea salt and DMS, and this would act as a negative climate feedback by increasing both the Arctic AOD and number concentration of cloud condensation nuclei.
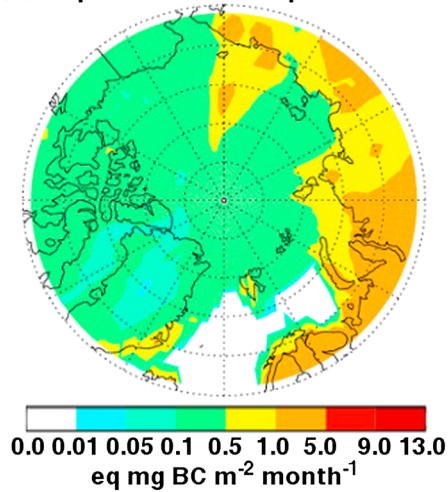
5. Absorption Aerosol Optical Depth and Deposition to Snow

In this section we quantify the relative contributions of absorbing aerosols (BC, OC, and dust) to the Arctic absorption aerosol optical depth (AAOD) at 550 nm and the deposition to Arctic snow and ice surfaces. The AAOD provides a measure of the total absorption of radiation at a given wavelength in the atmospheric column. The absorption by each species is calculated by multiplying the simulated column concentrations in grams per square meter by the mass absorption efficiency (MAE) at 550 nm. We use MAEs for BC and OC of $9.5\,m^2\,g^{-1}$ and $0.27\,m^2\,g^{-1}$, respectively, based on ARCTAS data [*McNaughton et al.*, 2011] and $0.03\,m^2\,g^{-1}$ for dust assuming a refractive index for dust of $1.53–0.0023i$ at 550 nm [*Yang et al.*, 2009]. The BC MAE estimate is for dry aerosol (RH < 40%) observed in the atmospheric environment and includes any enhancements due to coatings [*McNaughton et al.*, 2011]. We do not compare to AERONET AAOD observations in the Arctic because the single scattering albedo retrieval is not sufficiently sensitive when the AOD at 440 nm is below 0.4 [*Eck et al.*, 2009], which severely limits the available data.
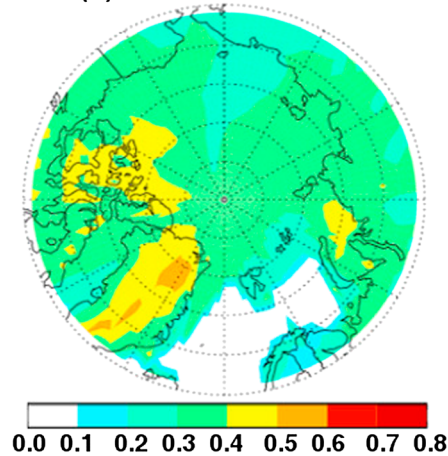
Figure 9b shows the simulated seasonality of area weighted Arctic AAOD. We find an annual mean Arctic AAOD of 0.004 with relative contributions of 80% from BC, 12% from OC, and 8% from dust. Maximum AAOD is in May because of large emissions of BC and OC from Russian fires, with a small additional contribution from dust. The secondary July maximum is attributable to fires. The largest non-BC fraction is simulated in spring because of the combination of fires and dust transport to the Arctic. Anthropogenic sources mainly from fuel combustion account for 46% of the annual Arctic AAOD, and fires account for 44% through contributions from both BC and OC.

The deposition of BC to high albedo surfaces in the Arctic has been estimated to contribute 20% of the twentieth century Arctic warming and snow ice cover loss [*Koch et al.*, 2011]. We calculate the deposition of BC to Arctic snow and ice surfaces during 2008 and quantify its relative importance compared to OC and dust. Figure 10a shows the simulated total deposition of BC, OC, and dust in equivalent grams of BC per month, providing a measure of the monthly mean deposited absorbing aerosol mass (DAM) in 2008. The equivalent BC flux is calculated by multiplying the simulated species deposition fluxes in kilograms per square meter per month by the ratio of the species MAE to the BC MAE as described for AAOD. We limit our

(a) Deposition Absorption Mass

0.0 0.01 0.05 0.1 0.5 1.0 5.0 9.0 13.0
eq mg BC m^{-2} month^{-1}

(b) Non-BC Fraction

0.0 0.1 0.2 0.3 0.4 0.5 0.6 0.7 0.8

Figure 10. (a) Total deposited absorption mass (DAM) of BC, OC, and dust to Arctic snow and ice surfaces in 2008, assuming MAE estimates at 550 nm in equivalent grams of BC per month. (b) Non-BC fraction. Values are GEOS-Chem model results for 2008. White areas are ice free year-round.

calculation in each month to surface grid squares that have a sea ice or land ice coverage greater than 50% or have a snow depth greater than 5 cm according to GEOS-5 meteorological fields. The total DAM is less than 0.5 eq mg BC m^{-2} month^{-1} in most of the Arctic. DAM fluxes are a factor of 3 higher in the Eurasian Arctic than the North American Arctic. The area of high DAM from Northern Siberia resulted from boreal fires emissions in Siberia in July.

Doherty et al. [2010] collected Arctic snow samples during 1998 and 2005–2009 and analyzed their light-absorbing properties. As in *Wang et al.* [2011], the spatial pattern of our simulated Arctic springtime BC snow concentrations is comparable to the observed pattern in *Doherty et al.* [2010]. Figure 10b shows that non-BC aerosol contributed 35% of the total DAM and up to 40–60% over Greenland, consistent with observations in *Doherty et al.* [2010], who found a non-BC fraction there of $55 \pm 8\%$. We attribute the large non-BC fraction over Greenland to the higher altitude favoring dust over BC. Source attribution shows that anthropogenic emissions contribute 85% of Arctic DAM in winter, while open fires contribute 47% in spring and 67% in summer. Dust deposition contributes 25% of DAM in spring and 10% in summer. Our results for the source attribution of DAM in the Arctic are consistent with the observations reported in *Hegg et al.* [2010], who determined that anthropogenic sources are the principal source of light-absorbing aerosol to Arctic snow in the winter and late autumn, while open-fire sources are most important in spring.

6. Discussion and Conclusions

We used the GEOS-Chem chemical transport model to simulate the distributions of aerosols and tropospheric ozone over the Arctic and separate the contributions from natural and anthropogenic sources. Our goal was to provide a credible representation of these near-term climate forcers to better understand their role in Arctic warming over the past decades. Our primary focus was on aerosols and the resulting aerosol optical depth (AOD) and absorption aerosol optical depth (AAOD). Comparisons were presented to 2008 observations from aircraft (ARCTAS), surface sites (including AERONET), and ship cruises, and also to multiyear surface and AERONET records. Our work provides the foundation for application of GEOS-Chem to long-term trends (1980–2010) of aerosols and ozone over the Arctic and for the accounting of these trends in climate models. This will be reported in later papers.

Previous applications of GEOS-Chem to simulate BC, OC, and sulfate aerosol during IPY had focused on the winter-spring period [*Fisher et al.*, 2011; *Wang et al.*, 2011]. Here we extended the analysis to the full year and separated natural and anthropogenic influences in order to distinguish radiative forcing from feedbacks. BC and sulfate peak in winter-spring and are minimum in summer-fall, and this is well captured by the model except for excessive BC at high altitudes in summer. The seasonal variation is largely driven by inflow of midlatitudes pollution and scavenging efficiency [*Shaw*, 1995; *Stohl*, 2006; *Matsui et al.*, 2011]. Most of BC is anthropogenic from fuel combustion throughout the year (58%), while sulfate is mostly anthropogenic in winter and spring but from natural sources (ocean and volcanoes) in summer and fall.

Analysis of the contribution of different geopolitical regions to Arctic BC shows that emissions from East Asia and Siberia (east of 75°E) are the most important source of anthropogenic BC in the Arctic, accounting for

30% of the Arctic troposphere BC burden. Europe and West Russia (15°W eastward to 75°E) together contribute 19% of the anthropogenic BC burden in the Arctic, while North America accounts for just 4%. These anthropogenic source contributions for Arctic BC in 2008 in our study are in good agreement with *Bourgeois and Bey* [2011].

Most of the OC aerosol in the Arctic atmosphere in spring and summer originates from boreal fires. The ARCTAS observations show a factor of 2 decrease in OC concentrations through much of the troposphere from spring to summer, and the model has similar results. However, surface observations in the high Arctic show a factor of 5 decrease from spring to summer that the model does not capture, suggesting model errors in scavenging or the need to account for lofting of fire plumes.

Little attention has been paid previously to dust in the Arctic, but we find it to be an important component of the aerosol in spring, with a dominant Saharan source. The ARCTAS observations further suggest a significant North American source of dust over the Arctic in summer, but this is not captured by the model.

The AOD observations from the AERONET network at Arctic sites (April–September) show an April maximum (0.14 across sites) and a June-July minimum (0.06). The model reproduces this seasonal variation and finds much larger AODs in the Eurasian Arctic, where AERONET observations are few, than in the North American Arctic. Additional AERONET stations are required in the central and eastern Eurasian Arctic to better constrain pan-Arctic AOD. We find that reproducing the observed AOD decrease from spring to summer in the model is critically contingent on accounting for the smaller particle size of sulfate in summer [*Quinn et al.*, 2002; *Engvall et al.*, 2008]. The model AOD is minimum in November–January, when no AERONET observations are available.

We used the model to analyze the major sources contributing to AOD at 550 nm in the Arctic. Sulfate accounts for 50% of AOD in spring and is then principally anthropogenic. Fires are the major source of Arctic AOD in summer. Volcanic eruptions can also make significant contributions (as the Kasatochi volcano did in August 2008). Sea salt is a major component in fall and winter, but the AOD is then low. Dust makes a 10% contribution to the spring maximum and is less important in other seasons. Most of the Arctic AOD is natural in all seasons (67% on an annual mean basis). The anthropogenic influence is largest in spring, contributing 0.06 AOD units then, mainly as sulfate.

Our simulations suggest a significant role not just for BC but also for OC and dust in shortwave absorption both in the snowpack and in the atmosphere. The deposited absorbing mass (DAM) to the Arctic snowpack in the model shows a non-BC contribution of 30–40% over the high Arctic and 40–60% over Greenland, consistent with observations by *Doherty et al.* [2010] and *Hegg et al.* [2010]. Light absorption by non-BC components in spring and summer contributes 24% of AAOD at 550 nm and 37% of DAM (in BC equivalent) over the scale of the Arctic. Fires were the dominant contributor to AAOD at 550 nm and DAM in 2008 because this was a high fire year; under normal fire conditions anthropogenic sources would likely dominate.

References

Alexander, B., R. J. Park, D. J. Jacob, Q. B. Li, R. M. Yantosca, J. Savarino, C. C. W. Lee, and M. H. Thiemens (2005), Sulfate formation in sea-salt aerosols: Constraints from oxygen isotopes, *J. Geophys. Res.*, 110, D10307, doi:10.1029/2004JD005659.

Alexander, B., R. J. Park, D. J. Jacob, and S. Gong (2009), Transition metal-catalyzed oxidation of atmospheric sulfur: Global implications for the sulfur budget, *J. Geophys. Res.*, 114, D02309, doi:10.1029/2008JD010486.

Alexander, B., D. J. Allman, H. M. Amos, T. D. Fairlie, J. Dachs, D. A. Hegg, and R. S. Sletten (2012), Isotopic constraints on the formation pathways of sulfate aerosol in the marine boundary layer of the subtropical northeast Atlantic Ocean, *J. Geophys. Res.*, 117, D06304, doi:10.1029/2011JD016773.

Alvarado, M. J., J. A. Logan, J. Mao, E. Apel, D. Riemer, D. Blake, R. C. Cohen, K.-E. Min, A. E. Perring, and E. C. Browne (2010), Nitrogen oxides and PAN in plumes from boreal fires during ARCTAS-B and their impact on ozone: An integrated analysis of aircraft and satellite observations, *Atmos. Chem. Phys.*, 10(20), 9739–9760.

Ansmann, A., et al. (2003), Long-range transport of Saharan dust to northern Europe: The 11–16 October 2001 outbreak observed with EARLINET, *J. Geophys. Res.*, 108(D24), 4783, doi:10.1029/2003JD003757.

Barnes, I., J. Hjorth, and N. Mihalopoulos (2006), Dimethyl sulfide and dimethyl sulfoxide and their oxidation in the atmosphere, *Chem. Rev.*, 106(3), 940–975.

Bodhaine, B. A., J. M. Harris, and G. A. Herbert (1981), Aerosol light scattering and condensation nuclei measurements at Barrow, Alaska, *Atmos. Environ. 1967*, 15(8), 1375–1389, doi:10.1016/0004-6981(81)90344-9.

Bond, T. C., D. G. Streets, K. F. Yarber, S. M. Nelson, J.-H. Woo, and Z. Klimont (2004), A technology-based global inventory of black and organic carbon emissions from combustion, *J. Geophys. Res.*, 109, D14203, doi:10.1029/2003JD003697.

Bond, T. C., E. Bhardwaj, R. Dong, R. Jogani, S. Jung, C. Roden, D. G. Streets, and N. M. Trautmann (2007), Historical emissions of black and organic carbon aerosol from energy-related combustion, 1850–2000, *Global Biogeochem. Cycles*, 21, GB2018, doi:10.1029/2006GB002840.

Bory, A.-M., P. E. Biscaye, A. M. Piotrowski, and J. P. Steffensen (2003), Regional variability of ice core dust composition and provenance in Greenland, *Geochem. Geophys. Geosyst.*, 4(12), 1107, doi:10.1029/2003GC000627.

Bourgeois, Q., and I. Bey (2011), Pollution transport efficiency toward the Arctic: Sensitivity to aerosol scavenging and source regions, *J. Geophys. Res.*, *116*, D08213, doi:10.1029/2010JD015096.

Browell, E. V., et al. (2003), Ozone, aerosol, potential vorticity, and trace gas trends observed at high-latitudes over North America from February to May 2000, *J. Geophys. Res.*, *108*(D4), 8369, doi:10.1029/2001JD001390.

Chang, R. Y.-W., et al. (2011), Aerosol composition and sources in the central Arctic Ocean during ASCOS, *Atmos. Chem. Phys.*, *11*(20), 10,619–10,636, doi:10.5194/acp-11-10619-2011.

Charlson, R. J., S. E. Schwartz, J. M. Hales, R. D. Cess, J. A. Coakley, J. E. Hansen, and D. J. Hofmann (1992), Climate forcing by anthropogenic aerosols, *Science*, *255*(5043), 423–430, doi:10.1126/science.255.5043.423.

Clarke, A. D., and K. J. Noone (1985), Soot in the Arctic snowpack: A cause for perturbations in radiative transfer, *Atmos. Environ. 1967*, *19*(12), 2045–2053, doi:10.1016/0004-6981(85)90113-1.

Dibb, J. E., R. W. Talbot, E. M. Scheuer, G. Seid, M. A. Avery, and H. B. Singh (2003), Aerosol chemical composition in Asian continental outflow during the TRACE-P campaign: Comparison with PEM-West B, *J. Geophys. Res.*, *108*(D21), 8815, doi:10.1029/2002JD003111.

Doherty, S. J., S. G. Warren, T. C. Grenfell, A. D. Clarke, and R. E. Brandt (2010), Light-absorbing impurities in Arctic snow, *Atmos. Chem. Phys.*, *10*(23), 11,647–11,680, doi:10.5194/acp-10-11647-2010.

Drury, E., D. J. Jacob, R. J. D. Spurr, J. Wang, Y. Shinozuka, B. E. Anderson, A. D. Clarke, J. Dibb, C. McNaughton, and R. Weber (2010), Synthesis of satellite (MODIS), aircraft (ICARTT), and surface (IMPROVE, EPA-AQS, AERONET) aerosol observations over eastern North America to improve MODIS aerosol retrievals and constrain surface aerosol concentrations and sources, *J. Geophys. Res.*, *115*, D14204, doi:10.1029/2009JD012629.

Eck, T. F., et al. (2009), Optical properties of boreal region biomass burning aerosols in central Alaska and seasonal variation of aerosol optical depth at an Arctic coastal site, *J. Geophys. Res.*, *114*, D11201, doi:10.1029/2008JD010870.

Eleftheriadis, K., S. Vratolis, and S. Nyeki (2009), Aerosol black carbon in the European Arctic: Measurements at Zeppelin station, Ny-Ålesund, Svalbard from 1998–2007, *Geophys. Res. Lett.*, *36*, L02809, doi:10.1029/2008GL035741.

Engvall, A.-C., R. Krejci, J. Ström, R. Treffeisen, R. Scheele, O. Hermansen, and J. Paatero (2008), Changes in aerosol properties during spring-summer period in the Arctic troposphere, *Atmos. Chem. Phys.*, *8*(3), 445–462, doi:10.5194/acp-8-445-2008.

Fairlie, T. D., D. J. Jacob, and R. J. Park (2007), The impact of transpacific transport of mineral dust in the United States, *Atmos. Environ.*, *41*(6), 1251–1266, doi:10.1016/j.atmosenv.2006.09.048.

Fairlie, T. D., D. J. Jacob, J. E. Dibb, B. Alexander, M. A. Avery, A. van Donkelaar, and L. Zhang (2010), Impact of mineral dust on nitrate, sulfate, and ozone in transpacific Asian pollution plumes, *Atmos. Chem. Phys.*, *10*(8), 3999–4012, doi:10.5194/acp-10-3999-2010.

Feng, J. (2007), A 3-mode parameterization of below-cloud scavenging of aerosols for use in atmospheric dispersion models, *Atmos. Environ.*, *41*(32), 6808–6822, doi:10.1016/j.atmosenv.2007.04.046.

Feng, J. (2009), A size-resolved model for below-cloud scavenging of aerosols by snowfall, *J. Geophys. Res.*, *114*, D08203, doi:10.1029/2008JD011012.

Fisher, J. A., D. J. Jacob, M. T. Purdy, M. Kopacz, P. L. Sager, C. Carouge, C. D. Holmes, R. M. Yantosca, R. L. Batchelor, and K. Strong (2010), Source attribution and interannual variability of Arctic pollution in spring constrained by aircraft (ARCTAS, ARCPAC) and satellite (AIRS) observations of carbon monoxide, *Atmos. Chem. Phys.*, *10*(3), 977–996.

Fisher, J. A., et al. (2011), Sources, distribution, and acidity of sulfate–ammonium aerosol in the Arctic in winter–spring, *Atmos. Environ.*, *45*(39), 7301–7318, doi:10.1016/j.atmosenv.2011.08.030.

Flanner, M. G., C. S. Zender, J. T. Randerson, and P. J. Rasch (2007), Present-day climate forcing and response from black carbon in snow, *J. Geophys. Res.*, *112*, D11202, doi:10.1029/2006JD008003.

Franzén, L. G., J. O. Mattsson, U. Maartensson, T. Nihlén, and A. Rapp (1994), Yellow snow over the Alps and subarctic from dust storm in Africa, March 1991, *Ambio*, 233–235.

Frossard, A. A., P. M. Shaw, L. M. Russell, J. H. Kroll, M. R. Canagaratna, D. R. Worsnop, P. K. Quinn, and T. S. Bates (2011), Springtime Arctic haze contributions of submicron organic particles from European and Asian combustion sources, *J. Geophys. Res.*, *116*, D05205, doi:10.1029/2010JD015178.

Fu, T.-M., D. J. Jacob, F. Wittrock, J. P. Burrows, M. Vrekoussis, and D. K. Henze (2008), Global budgets of atmospheric glyoxal and methylglyoxal, and implications for formation of secondary organic aerosols, *J. Geophys. Res.*, *113*, D15303, doi:10.1029/2007JD009505.

Fu, T.-M., D. J. Jacob, and C. L. Heald (2009), Aqueous-phase reactive uptake of dicarbonyls as a source of organic aerosol over eastern North America, *Atmos. Environ.*, *43*(10), 1814–1822.

Ginoux, P., M. Chin, I. Tegen, J. M. Prospero, B. Holben, O. Dubovik, and S.-J. Lin (2001), Sources and distributions of dust aerosols simulated with the GOCART model, *J. Geophys. Res.*, *106*(D17), 20,255–20,273, doi:10.1029/2000JD000053.

Gong, S. L., T. L. Zhao, S. Sharma, D. Toom-Sauntry, D. Lavoué, X. B. Zhang, W. R. Leaitch, and L. A. Barrie (2010), Identification of trends and interannual variability of sulfate and black carbon in the Canadian High Arctic: 1981–2007, *J. Geophys. Res.*, *115*, D07305, doi:10.1029/2009JD012943.

Hansen, J., and L. Nazarenko (2004), Soot climate forcing via snow and ice albedos, *Proc. Natl. Acad. Sci. U.S.A.*, *101*(2), 423–428, doi:10.1073/pnas.2237157100.

Hegg, D. A., S. G. Warren, T. C. Grenfell, S. J. Doherty, and A. D. Clarke (2010), Sources of light-absorbing aerosol in arctic snow and their seasonal variation, *Atmos. Chem. Phys.*, *10*(22), 10,923–10,938, doi:10.5194/acp-10-10923-2010.

Henze, D. K., and J. H. Seinfeld (2006), Global secondary organic aerosol from isoprene oxidation, *Geophys. Res. Lett.*, *33*, L09812, doi:10.1029/2006GL025976.

Hirdman, D., H. Sodemann, S. Eckhardt, J. F. Burkhart, A. Jefferson, T. Mefford, P. K. Quinn, S. Sharma, J. Ström, and A. Stohl (2010), Source identification of short-lived air pollutants in the Arctic using statistical analysis of measurement data and particle dispersion model output, *Atmos. Chem. Phys.*, *10*(2), 669–693, doi:10.5194/acp-10-669-2010.

Hoffmann, A., C. Ritter, M. Stock, M. Maturilli, S. Eckhardt, A. Herber, and R. Neuber (2010), Lidar measurements of the Kasatochi aerosol plume in August and September 2008 in Ny-Ålesund, Spitsbergen, *J. Geophys. Res.*, *115*, D00L12, doi:10.1029/2009JD013039.

Holben, B. N., et al. (1998), AERONET—A federated instrument network and data archive for aerosol characterization, *Remote Sens. Environ.*, *66*(1), 1–16, doi:10.1016/S0034-4257(98)00031-5.

Hudman, R. C., L. T. Murray, D. J. Jacob, D. B. Millet, S. Turquety, S. Wu, D. R. Blake, A. H. Goldstein, J. Holloway, and G. W. Sachse (2008), Biogenic versus anthropogenic sources of CO in the United States, *Geophys. Res. Lett.*, *35*, L04801, doi:10.1029/2007GL032393.

Hyvärinen, A.-P., et al. (2011), Aerosol black carbon at five background measurement sites over Finland, a gateway to the Arctic, *Atmos. Environ.*, *45*(24), 4042–4050, doi:10.1016/j.atmosenv.2011.04.026.

Jacob, D. J., J. H. Crawford, H. Maring, A. D. Clarke, J. E. Dibb, L. K. Emmons, R. A. Ferrare, C. A. Hostetler, P. B. Russell, and H. B. Singh (2010), The arctic research of the composition of the troposphere from aircraft and satellites (ARCTAS) mission: Design, execution, and first results, *Atmos. Chem. Phys.*, *10*(11), 5191–5212.

Jimenez, J. L., et al. (2003), Ambient aerosol sampling using the Aerodyne Aerosol Mass Spectrometer, *J. Geophys. Res.*, *108*(D7), 8425, doi:10.1029/2001JD001213.

Koch, D., et al. (2009), Evaluation of black carbon estimations in global aerosol models, *Atmos. Chem. Phys.*, *9*(22), 9001–9026, doi:10.5194/acp-9-9001-2009.

Koch, D., et al. (2011), Coupled aerosol-chemistry–climate twentieth-century transient model investigation: Trends in short-lived species and climate responses, *J. Clim.*, *24*(11), 2693–2714, doi:10.1175/2011JCLI3582.1.

Kondo, Y., et al. (2011), Emissions of black carbon, organic, and inorganic aerosols from biomass burning in North America and Asia in 2008, *J. Geophys. Res.*, *116*, D08204, doi:10.1029/2010JD015152.

Kravitz, B., A. Robock, and A. Bourassa (2010), Negligible climatic effects from the 2008 Okmok and Kasatochi volcanic eruptions, *J. Geophys. Res.*, *115*, D00L05, doi:10.1029/2009JD013525.

Lana, A., et al. (2011), An updated climatology of surface dimethlysulfide concentrations and emission fluxes in the global ocean, *Global Biogeochem. Cylces*, *25*, GB1004, doi:10.1029/2010GB003850.

Law, K. S., and A. Stohl (2007), Arctic air pollution: Origins and impacts, *Science*, *315*(5818), 1537–1540, doi:10.1126/science.1137695.

Lazaridis, M., A. Semb, S. Larssen, A.-G. Hjellbrekke, Ø. Hov, J. E. Hanssen, J. Schaug, and K. Tørseth (2002), Measurements of particulate matter within the framework of the European Monitoring and Evaluation Programme (EMEP): I. First results, *Sci. Total Environ.*, *285*(1), 209–235.

Lu, Z., Q. Zhang, and D. G. Streets (2011), Sulfur dioxide and primary carbonaceous aerosol emissions in China and India, 1996–2010, *Atmos. Chem. Phys.*, *11*(18), 9839–9864, doi:10.5194/acp-11-9839-2011.

Malm, W. C., J. F. Sisler, D. Huffman, R. A. Eldred, and T. A. Cahill (1994), Spatial and seasonal trends in particle concentration and optical extinction in the United States, *J. Geophys. Res.*, *99*(D1), 1347–1370, doi:10.1029/93JD02916.

Malm, W. C., B. A. Schichtel, M. L. Pitchford, L. L. Ashbaugh, and R. A. Eldred (2004), Spatial and monthly trends in speciated fine particle concentration in the United States, *J. Geophys. Res.*, *109*, D03306, doi:10.1029/2003JD003739.

Mao, J., et al. (2010), Chemistry of hydrogen oxide radicals (HO_x) in the Arctic troposphere in spring, *Atmos. Chem. Phys.*, *10*(13), 5823–5838, doi:10.5194/acp-10-5823-2010.

Matsui, H., Y. Kondo, N. Moteki, N. Takegawa, L. K. Sahu, Y. Zhao, H. E. Fuelberg, W. R. Sessions, G. Diskin, and D. R. Blake (2011), Seasonal variation of the transport of black carbon aerosol from the Asian continent to the Arctic during the ARCTAS aircraft campaign, *J. Geophys. Res.*, *116*, D05202, doi:10.1029/2010JD015067.

McNaughton, C. S., et al. (2011), Absorbing aerosol in the troposphere of the Western Arctic during the 2008 ARCTAS/ARCPAC airborne field campaigns, *Atmos. Chem. Phys.*, *11*(15), 7561–7582, doi:10.5194/acp-11-7561-2011.

Meier, W. N., J. Stroeve, and F. Fetterer (2007), Whither Arctic sea ice? A clear signal of decline regionally, seasonally and extending beyond the satellite record, *Ann. Glaciol.*, *46*(1), 428–434, doi:10.3189/172756407782871170.

Mickley, L. J., P. P. Murti, D. J. Jacob, J. A. Logan, D. M. Koch, and D. Rind (1999), Radiative forcing from tropospheric ozone calculated with a unified chemistry-climate model, *J. Geophys. Res.*, *104*(D23), 30,153–30,172.

Mickley, L. J., D. J. Jacob, B. D. Field, and D. Rind (2004), Climate response to the increase in tropospheric ozone since preindustrial times: A comparison between ozone and equivalent CO_2 forcings, *J. Geophys. Res.*, *109*, D05106, doi:10.1029/2003JD003653.

Mitchell, M. (1956), Visual range in the polar regions with particular reference to the Alaskan Arctic, *J. Atmos. Terr. Phys. Spec. Suppl.*, 195–211.

Nilsson, E. D., and Ü. Rannik (2001), Turbulent aerosol fluxes over the Arctic Ocean: 1. Dry deposition over sea and pack ice, *J. Geophys. Res.*, *106*(D23), 32,125–32,137, doi:10.1029/2000JD900605.

Oltmans, S. J., A. S. Lefohn, J. M. Harris, I. Galbally, H. E. Scheel, G. Bodeker, E. Brunke, H. Claude, D. Tarasick, and B. J. Johnson (2006), Long-term changes in tropospheric ozone, *Atmos. Environ.*, *40*(17), 3156–3173.

Perry, K. D., T. A. Cahill, R. A. Eldred, D. D. Dutcher, and T. E. Gill (1997), Long-range transport of North African dust to the eastern United States, *J. Geophys. Res.*, *102*(D10), 11,225–11,238, doi:10.1029/97JD00260.

Quinn, P. K., et al. (2000), Surface submicron aerosol chemical composition: What fraction is not sulfate?, *J. Geophys. Res.*, *105*(D5), 6785–6805, doi:10.1029/1999JD901034.

Quinn, P. K., T. L. Miller, T. S. Bates, J. A. Ogren, E. Andrews, and G. E. Shaw (2002), A 3-year record of simultaneously measured aerosol chemical and optical properties at Barrow, Alaska, *J. Geophys. Res.*, *107*(D11), 4130, doi:10.1029/2001JD001248.

Quinn, P. K., G. Shaw, E. Andrews, E. G. Dutton, T. Ruoho-Airola, and S. L. Gong (2007), Arctic haze: Current trends and knowledge gaps, *Tellus B*, *59*(1), 99–114, doi:10.1111/j.1600-0889.2006.00238.x.

Quinn, P. K., et al. (2008), Short-lived pollutants in the Arctic: Their climate impact and possible mitigation strategies, *Atmos. Chem. Phys.*, *8*(6), 1723–1735, doi:10.5194/acp-8-1723-2008.

Radke, L. F., P. V. Hobbs, and I. H. Bailey (1984), Airborne observations of Arctic aerosols, III: Origins and effects of airmasses, *Geophys Res. Lett.*, *11*(5), 401–404.

Rahn, K. A. (1981), Relative importances of North America and Eurasia as sources of Arctic aerosol, *Atmos. Environ.*, *15*(8), 1447–1455.

Rahn, K. A., and R. J. McCaffrey (1980), On the origin and transport of the winter Arctic aerosol, *Annu. N. Y. Acad. Sci.*, *338*, 486–503.

Reid, J. S., et al. (2009), Global monitoring and forecasting of biomass-burning smoke: Description of and lessons from the Fire Locating and Modeling of Burning Emissions (FLAMBE) program, *IEEE J. Sel. Top. Appl. Earth Obs. Remote Sens.*, *2*(3), 144–162, doi:10.1109/JSTARS.2009.2027443.

Ridley, D. A., C. L. Heald, and B. Ford (2012), North African dust export and deposition: A satellite and model perspective, *J. Geophys. Res.*, *117*, D02202, doi:10.1029/2011JD016794.

Rodríguez, E., C. Toledano, V. E. Cachorro, P. Ortiz, K. Stebel, A. Berjón, S. Blindheim, M. Gausa, and A. M. de Frutos (2012), Aerosol characterization at the sub-Arctic site Andenes (69°N, 16°E), by the analysis of columnar optical properties, *Q. J. R. Meteorol. Soc.*, *138*(663), 471–482, doi:10.1002/qj.921.

Seinfeld, J. H., and S. N. Pandis (2006), *Atmospheric Chemistry and Physics: From Air Pollution to Climate Change*, John Wiley, Hoboken, N. J.

Sharma, S., M. Ishizawa, D. Chan, D. Lavoué, E. Andrews, K. Eleftheriadis, and S. Maksyutov (2013), 16-year simulation of Arctic black carbon: Transport, source contribution, and sensitivity analysis on deposition, *J. Geophys. Res. Atmos.*, *118*, 943–964, doi:10.1029/2012JD017774.

Shaw, G. E. (1995), The Arctic haze phenomenon, *Bull. Am. Meteorol. Soc.*, *76*(12), 2403–2413, doi:10.1175/1520-0477(1995)076<2403: TAHP>2.0.CO;2.

Shaw, P. M., L. M. Russell, A. Jefferson, and P. K. Quinn (2010), Arctic organic aerosol measurements show particles from mixed combustion in spring haze and from frost flowers in winter, *Geophys. Res. Lett.*, *37*, L10803, doi:10.1029/2010GL042831.

Shindell, D., and G. Faluvegi (2009), Climate response to regional radiative forcing during the twentieth century, *Nat. Geosci.*, *2*(4), 294–300, doi:10.1038/ngeo473.

Shindell, D., G. Faluvegi, A. Lacis, J. Hansen, R. Ruedy, and E. Aguilar (2006), Role of tropospheric ozone increases in 20th-century climate change, *J. Geophys. Res.*, *111*, D08302, doi:10.1029/2005JD006348.

Shindell, D. T., G. Faluvegi, S. E. Bauer, D. M. Koch, N. Unger, S. Menon, R. L. Miller, G. A. Schmidt, and D. G. Streets (2007), Climate response to projected changes in short-lived species under an A1B scenario from 2000–2050 in the GISS climate model, *J. Geophys. Res.*, *112*, D20103, doi:10.1029/2007JD008753.

Shindell, D. T., M. Chin, F. Dentener, R. M. Doherty, G. Faluvegi, A. M. Fiore, P. Hess, D. M. Koch, I. A. MacKenzie, and M. G. Sanderson (2008), A multi-model assessment of pollution transport to the Arctic, *Atmos. Chem. Phys.*, *8*(17), 5353–5372.

Smith, S. J., J. van Aardenne, Z. Klimont, R. J. Andres, A. Volke, and S. Delgado Arias (2011), Anthropogenic sulfur dioxide emissions: 1850–2005, *Atmos. Chem. Phys.*, *11*(3), 1101–1116, doi:10.5194/acp-11-1101-2011.

Song, C. H., and G. R. Carmichael (2001), Gas-particle partitioning of nitric acid modulated by alkaline aerosol, *J. Atmos. Chem.*, *40*(1), 1–22, doi:10.1023/A:1010657929716.

Stohl, A. (2006), Characteristics of atmospheric transport into the Arctic troposphere, *J. Geophys. Res.*, *111*, D11306, doi:10.1029/2005JD006888.

Stroeve, J., M. M. Holland, W. Meier, T. Scambos, and M. Serreze (2007), Arctic sea ice decline: Faster than forecast, *Geophys. Res. Lett.*, *34*, L09501, doi:10.1029/2007GL029703.

Ström, J., J. Umegård, K. Tørseth, P. Tunved, H.-C. Hansson, K. Holmén, V. Wismann, A. Herber, and G. König-Langlo (2003), One year of particle size distribution and aerosol chemical composition measurements at the Zeppelin Station, Svalbard, March 2000–March 2001, *Phys. Chem. Earth Parts ABC*, *28*(28–32), 1181–1190, doi:10.1016/j.pce.2003.08.058.

Talbot, R. W., J. E. Dibb, and M. B. Loomis (1998), Influence of vertical transport on free tropospheric aerosols over the central USA in springtime, *Geophys. Res. Lett.*, *25*(9), 1367–1370, doi:10.1029/98GL00184.

Tomasi, C., et al. (2012), An update on polar aerosol optical properties using POLAR-AOD and other measurements performed during the International Polar Year, *Atmos. Environ.*, *52*, 29–47, doi:10.1016/j.atmosenv.2012.02.055.

Trenberth, K. E., P. D. Jones, P. Ambenje, R. Bojariu, D. Easterling, A. K. Tank, D. Parker, F. Rahimzadeh, J. A. Renwick, and M. Rusticucci (2007), Observations: Surface and atmospheric climate change, chap. 3 of Climate Change 2007: The Physical Science Basis, in *Contribution of Working Group I to the Fourth Assessment Report of the Intergovernmental Panel on Climate Change*, edited by S. Solomon et al., pp. 235–336, Cambridge Univ. Press, Cambridge, U. K., and New York.

Turpin, B. J., and H.-J. Lim (2001), Species contributions to PM2. 5 mass concentrations: Revisiting common assumptions for estimating organic mass, *Aerosol Sci. Technol.*, *35*(1), 602–610.

Twomey, S. (1974), Pollution and the planetary albedo, *Atmos. Environ. 1967*, *8*(12), 1251–1256, doi:10.1016/0004-6981(74)90004-3.

VanCuren, R. A., T. Cahill, J. Burkhart, D. Barnes, Y. Zhao, K. Perry, S. Cliff, and J. McConnell (2012), Aerosols and their sources at Summit Greenland—First results of continuous size- and time-resolved sampling, *Atmos. Environ.*, *52*, 82–97, doi:10.1016/j.atmosenv.2011.10.047.

Van Donkelaar, A., et al. (2008), Analysis of aircraft and satellite measurements from the Intercontinental Chemical Transport Experiment (INTEX-B) to quantify long-range transport of East Asian sulfur to Canada, *Atmos. Chem. Phys.*, *8*(11), 2999–3014, doi:10.5194/acp-8-2999-2008.

Wang, Q., et al. (2011), Sources of carbonaceous aerosols and deposited black carbon in the Arctic in winter-spring: Implications for radiative forcing, *Atmos. Chem. Phys.*, *11*(23), 12,453–12,473, doi:10.5194/acp-11-12453-2011.

Wang, Q., D. J. Jacob, J. R. Spackman, A. E. Perring, J. P. Schwarz, N. Moteki, E. A. Marais, C. Ge, J. Wang, and S. R. H. Barrett (2014), Global budget and radiative forcing of black carbon aerosol: Constraints from pole-to-pole (HIPPO) observations across the Pacific, *J. Geophys. Res. Atmos.*, *119*, 195–206, doi:10.1002/2013JD020824.

Warneke, C., et al. (2009), Biomass burning in Siberia and Kazakhstan as an important source for haze over the Alaskan Arctic in April 2008, *Geophys. Res. Lett.*, *36*, L02813, doi:10.1029/2008GL036194.

Warneke, C., et al. (2010), An important contribution to springtime Arctic aerosol from biomass burning in Russia, *Geophys. Res. Lett.*, *37*, L01801, doi:10.1029/2009GL041816.

Warren, S. G., and W. J. Wiscombe (1980), A model for the spectral albedo of snow, II: Snow containing atmospheric aerosols, *J. Atmos. Sci.*, *37*(12), 2734–2745, doi:10.1175/1520-0469(1980)037<2734:AMFTSA>2.0.CO;2.

Wesely, M. L. (1989), Parameterization of surface resistances to gaseous dry deposition in regional-scale numerical models, *Atmos. Environ.*, *23*, 1293–1304.

Yang, M., S. G. Howell, J. Zhuang, and B. J. Huebert (2009), Attribution of aerosol light absorption to black carbon, brown carbon, and dust in China—Interpretations of atmospheric measurements during EAST-AIRE, *Atmos. Chem. Phys.*, *9*(6), 2035–2050, doi:10.5194/acp-9-2035-2009.

Zender, C. S., H. Bian, and D. Newman (2003), Mineral Dust Entrainment and Deposition (DEAD) model: Description and 1990s dust climatology, *J. Geophys. Res.*, *108*(D14), 4416, doi:10.1029/2002JD002775.